Original Article

Malignant astrocyte swelling and impaired glutamate clearance drive the expansion of injurious spreading depolarization foci

Ákos Menyhárt[1],*, Rita Frank[1],*, Attila E Farkas[2], Zoltán Süle[3],
Viktória É Varga[1], Ádám Nyúl-Tóth[2,4], Anne Meiller[5],
Orsolya Ivánkovits-Kiss[1], Coline L Lemale[6,7], Írisz Szabó[1],
Réka Tóth[1], Dániel Zölei-Szénási[1], Johannes Woitzik[8],
Stephane Marinesco[5], István A Krizbai[2,9], Ferenc Bari[1],
Jens P Dreier[6,7,10,11,12] (iD) and Eszter Farkas[13,14] (iD)

Abstract

Spreading depolarizations (SDs) indicate injury progression and predict worse clinical outcome in acute brain injury. We demonstrate in rodents that acute brain swelling upon cerebral ischemia impairs astroglial glutamate clearance and increases the tissue area invaded by SD. The cytotoxic extracellular glutamate accumulation ($>15\,\mu M$) predisposes an extensive bulk of tissue (4–$5\,mm^2$) for a yet undescribed simultaneous depolarization (SiD). We confirm in rat brain slices exposed to osmotic stress that SiD is the pathological expansion of prior punctual SD foci (0.5–$1\,mm^2$), is associated with astrocyte swelling, and triggers oncotic neuron death. The blockade of astrocytic aquaporin-4 channels and $Na^+/K^+/Cl^-$ co-transporters, or volume-regulated anion channels mitigated slice edema, extracellular glutamate accumulation ($<10\,\mu M$) and SiD occurrence. Reversal of slice swelling by hyperosmotic mannitol counteracted glutamate accumulation and prevented SiD. In contrast, inhibition of glial metabolism or inhibition of astrocyte glutamate transporters reproduced the SiD phenotype. Finally, we show in the rodent water intoxication model of cytotoxic edema that astrocyte swelling and altered astrocyte calcium waves are central in the evolution of SiD. We discuss our

[1]Department of Medical Physics and Informatics, Faculty of Medicine and Faculty of Science and Informatics, University of Szeged, Szeged, Hungary
[2]Neurovascular Unit Research Group, Molecular Neurobiology Research Unit, Institute of Biophysics, Biological Research Centre, Szeged, Hungary
[3]Department of Anatomy, Histology and Embryology, Faculty of Medicine, University of Szeged, Szeged, Hungary
[4]Vascular Cognitive Impairment and Neurodegeneration Program, Reynolds Oklahoma Center on Aging/Oklahoma Center for Geroscience, Department of Biochemistry and Molecular Biology, University of Oklahoma Health Sciences Center, Oklahoma City, OK, USA
[5]Lyon Neuroscience Research Center, Inserm U1028, CNRS UMR 5292, University Claude Bernard Lyon I, Lyon, France
[6]Center for Stroke Research Berlin, Charité – Universitätsmedizin Berlin, Corporate Member of Freie Universität Berlin, Humboldt-Universität zu Berlin, and Berlin Institute of Health, Berlin, Germany
[7]Department of Experimental Neurology, Charité – Universitätsmedizin Berlin, Corporate Member of Freie Universität Berlin, Humboldt-Universität zu Berlin, and Berlin Institute of Health, Berlin, Germany
[8]Department of Neurosurgery, Charité – Universitätsmedizin Berlin, Corporate Member of Freie Universität Berlin, Humboldt-Universität zu Berlin, and Berlin Institute of Health, Berlin, Germany
[9]Institute of Life Sciences, Vasile Goldis Western University, Arad, Romania

[10]Department of Neurology, Charité – Universitätsmedizin Berlin, corporate member of Freie Universität Berlin, Humboldt-Universität zu Berlin, and Berlin Institute of Health, Berlin, Germany
[11]Bernstein Center for Computational Neuroscience Berlin, Berlin, Germany
[12]Einstein Center for Neurosciences Berlin, Berlin, Germany
[13]HCEMM-USZ Cerebral Blood Flow and Metabolism Research Group, Szeged, Hungary
[14]Department of Cell Biology and Molecular Medicine, Faculty of Medicine and Faculty of Science and Informatics, University of Szeged, Szeged, Hungary

*These authors contributed equally to this work.

Corresponding authors:
Ákos Menyhárt, Department of Medical Physics and Informatics, Faculty of Medicine, and Faculty of Science and Informatics, University of Szeged, Korányi fasor 9, H-6720 Szeged, Hungary.
Email: menyhartakos89@gmail.com

Eszter Farkas, Department of Medical Physics and Informatics, Faculty of Medicine, and Faculty of Science and Informatics, University of Szeged, Korányi fasor 9, H-6720 Szeged, Hungary.
Email: eszter.farkas.szeged@gmail.com

results in the light of evidence for SiD in the human cortex. Our results emphasize the need of preventive osmotherapy in acute brain injury.

Introduction

Cerebral edema is a key prognosticator of unfavorable outcome in acute ischemic, hemorrhagic or traumatic brain injury, in which spreading depolarizations (SDs) are implicated. Moreover, the robust correlate of lesion progression after acute brain injury is a characteristic pattern of SDs, which serves as an electrophysiological biomarker of injury progression, and is considered as a target of pharmacological intervention.[1–4] SD is a slowly propagating wave (2-6 mm/min) of a near complete cellular depolarization followed by the transient depression of neural activity and cytotoxic edema.[5–7] In addition to the cytotoxic water translocation within the nervous tissue, ischemic SD initiates cerebrospinal fluid influx and drives acute brain swelling after middle cerebral artery occlusion in mice.[8]

Although SD is primarily the profound ionic disturbance of neurons, intact astrocytic clearance mechanisms are essential for the recovery of the tissue from SD.[5] Under stress, the notable swelling of astroglia impairs K^+ and glutamate clearance, which makes neurons susceptible for increased action potential firing, epileptiform activity and SD, and compromises neuronal viability.[9–12] Moreover, astrocyte swelling in response to metabolic poisoning by fluorocitrate provoked spontaneous SD occurrence, and prolonged SD duration and neuronal injury in anesthetized rats.[13–15] In focal cerebral ischemia, the degree of astrocyte soma swelling was found coincident with the cumulative duration of recurrent SDs and dendritic beading.[16,17]

SD has been recognized to propagate from a punctual focus, yet the cellular mechanistic understanding of SD eruption is incomplete. The minimum tissue volume of the SD focus was estimated to be ~ 1 mm^3 *in vivo*, or even smaller, ~ 0.03–0.06 mm^3 *in vitro*.[3,18–20] In focal ischemia, this critical mass of tissue is localized to the inner penumbra, where instable or metastable hot zones created by metabolic supply-demand mismatch give rise to SD.[3,21] In these particular hot zones, astrocytic K^+ and glutamate uptake may be significantly arrested, which is expected to compel a contiguous group of equally exhausted, ATP depleted neurons to fail to maintain the resting ion gradients across their cell membrane, and lose their resting potential instantaneously.[22] This simultaneously depolarized, discrete tissue volume is suggested to correspond to the SD focus. The pathophysiological significance of the SD focus has remained poorly understood, because the focus of a spontaneous SD has been rarely captured due to its spatiotemporal unpredictability.[20,23]

Here we present novel observations in anesthetized rats that the simultaneously depolarized tissue volume denoting the focus of an SD event (i.e. simultaneous depolarization, SiD) may become extensive rather than punctual during acute ischemic tissue swelling. We demonstrate that malignant astrocyte swelling promotes SiD evolution and neuron death in our edema models. We further show that SiD encompasses tissue that has previously participated in the propagation of an SD, causing the subsequent aggravation of histological damage. Taken together our data demonstrate the intensified pathogenic potential of SD during acute edema formation.

Materials and methods

The procedures were approved by the National Food Chain Safety and Animal Health Directorate of Csongrád-Csanád County, Hungary, and performed according to the guidelines of the Scientific Committee of Animal Experimentation of the Hungarian Academy of Sciences (updated Law and Regulations on Animal Protection: 40/2013. (II. 14.) Gov. of Hungary), following the EU Directive 2010/63/EU on the protection of animals used for scientific purposes, and reported in compliance with the ARRIVE guidelines.[24]

Global forebrain ischemia/anoxia in anesthetized rats

Adult, male Sprague-Dawley rats (Charles River Laboratories, 365 ± 195 g, n = 23; electrophysiology and imaging: 18 rats, glutamate biosensors and

histology: 5 rats) were used. Surgical procedures, preparation of craniotomies, and ischemia induction were identical to those reported earlier (see Supplementary material).[25]

Electrophysiology and multimodal imaging. Local field potential (LFP) filtered in direct current (DC) potential mode and local changes of cerebral blood flow (CBF) were acquired at two distinct locations (4–4.5 mm inter-electrode distance) from the rostral craniotomy (see Supplementary material). Oxygen was withdrawn from the anesthetic gas mixture 50 min after ischemia induction to create an episode of anoxia, which produced anoxic/ischemic depolarization (recurrent SD: rSD, or simultaneous depolarization: SiD). The condition of anoxia was resolved by re-oxygenation 5 min later, followed by an additional 25 min of data acquisition. Intrinsic optical signal (IOS) imaging at green light illumination was performed as described previously, and detailed in the Supplement to this paper.[26,27]

Measurement of extra-synaptic glutamate concentration. Extra-synaptic glutamate concentrations were acquired using oxidase enzyme-based microelectrode biosensors (tip diameter: 30–40 μm; see Supplementary material for details) with constant potential amperometry.[28] Biosensors were calibrated before and after experiments in 0.01 M phosphate-buffered saline (PBS) with stepwise injections of glutamate concentration standards (5, 10, 15, 20, 25, 30, 35, 40, 45 μM). Glutamate oxidase enzyme sensitivity was confirmed by the application of 5 μM D-serine. During measurements, a constant potential of 500 mV was applied vs. an Ag/AgCl- electrode placed in the recording tissue chamber or under the skin of the animal's neck. Glutamate biosensors were lowered into the cortex together with LFP microelectrodes and control sensors covered with bovine serum albumin only (BSA, SigmaAldrich, St Quentin Fallavier, France) adjacent to the LFP microelectrodes together with glutamate null or BSA sensors. These control biosensors recorded negligible currents (glutamate independent) compared with glutamate biosensors. Biosensors were connected to a dedicated 3-electrode potentiostat (Quadstat) equipped with an eDAQ data acquisition system (eDAQ Pty Ltd., Colorado Springs, CO, USA) and a dedicated eDAQ Chart program.

Histology. Animals were transcardially perfused with physiological saline followed by 4% paraformaldehyde (PFA). The brains were removed and post-fixed in 4% PFA for 24 hours. Twenty-μm brain slices were cut with a freezing microtome after cryoprotection with 30% sucrose in PBS. Cleaved caspase-3 labeling was co-localized with the neuron marker NeuN or the astrocyte marker glial fibrillary acidic protein (GFAP). A detailed protocol for immunolabeling and image processing is given in the Supplement to this paper.

Nissl staining to visualize necrosis was carried out on 20 μm thick brain slices mounted on Superfrost+ slides in 0.3% polyvinyl-alcohol solution and dried at room temperature. Slides were incubated with 1% cresyl violet (containing 0.08% acetic acid) for 20 min at 50 °C, rinsed with distilled water, dehydrated, and mounted with Depex® mounting medium. The slides were examined under a Nikon Eclipse 80i brightfield microscope at 4× and 20× magnification, and images were captured with a camera (QImaging MicroPublisher) operated via ImagePro Plus software.

Hypo-osmotic cerebral edema model in anesthetized rats and mice

Water intoxication in anesthetized rats: Electrophysiology. Male Wistar rats (Charles River Laboratories, 2 months old, 250 ± 100 g, n = 15) were used. Anesthesia and surgical procedures (including craniotomy) are given in the Supplement to this paper, except for carotid artery preparation and occlusion. In brief, the rostral craniotomy incorporated two LFP electrodes, while the caudal craniotomy served SD elicitation. Hypo-osmotic brain edema was achieved by water intoxication imposed by the intraperitoneal injection of distilled water (DW; 15% body weight) (n = 6).[29] In the control group (n = 4) physiological saline was administered in the same volume as DW. In one rat, SD occurred spontaneously due to DW administration. In the other rats (n = 7), continuous SD elicitation was achieved by placing and leaving a 1 M KCl soaked cotton ball to the brain surface, 30 minutes after DW or physiological saline administration. In some rats (n = 2), KCl was washed out with aCSF after the occurrence of the first SD, and 30 min later O_2 was withdrawn from the anesthetic gas mixture.

To underscore the implication of edema formation in SiD, we attenuated edema by the administration of mannitol (2 mg/kg) to 4 rats through a catheter inserted to the femoral vein. In brief, 20 minutes after DW intoxication, mannitol was infused intravenously, then a KCl soaked cotton ball was placed into the caudal craniotomy as above. In 2 rats, KCl was washed out with aCSF after the first spreading depolarization (SD1) occurrence, while in other 2 rats, the cotton ball was left on the brain surface for continuous SD elicitation. After 30 minutes of data acquisition, rats were exposed to anoxia as described above.

MABP was monitored continuously, and arterial blood gases were checked regularly (i.e. during baseline, under ischemia, and under anoxia) via a catheter

inserted into the left femoral artery. Level of anesthesia was controlled with the aid of MABP displayed live as experiments were in progress.

Water intoxication in anesthetized mice: Two-photon imaging. Male C57BL/6 mice (8–10 weeks old, n = 10) were anesthetized with 1% Avertin (20 μL/g, i.p.), and mounted on a stereotactic frame incorporating a heating pad.[25] A cranial window (d = 3 mm) was prepared on the right parietal bone, and the dura was retracted. For astrocyte calcium imaging, the exposed brain surface was first loaded topically with a green fluorescent calcium indicator Fluo 4-AM (45 μM in aCSF, Thermo Fisher, Waltham, MA, USA) and incubated for 15 minutes. Subsequently, to monitor astrocyte swelling, the astrocyte specific non-fixable red fluorescent dye sulforhodamine 101 (SR-101, 80 μM in aCSF, Thermo Fisher, Waltham, MA, USA) was applied topically, and incubated for further 15 minutes. The craniotomy was then closed with a microscopic cover glass. Multiphoton excitation was performed at 810 nm wavelength according to the protocols described previously (Supplement to this paper).[25] Final imaging depth in the parietal cortex was 55–85 μm, where a z-stack with 5 μm vertical steps was recorded at the area of interest for identification of astrocytes. Image sequences were taken of the desired cells at approximately 200–400 nm/pixel spatial and 0.8–2.5 Hz temporal resolution. After baseline (5 min), mice received stepwise intraperitoneal DW injections (3 times 1.5 ml/10 minutes) to 15% volume of body weight. SD was then elicited with the topical application of 1 M KCl, and SD evolution was confirmed by the occurrence of synchronous astrocytic calcium waves (Fluo 4-AM intensity increase, green channel) and the associated volume changes of astrocyte soma and processes (SR-101 labeled soma volume changes, red channel).

Hypo-osmotic cerebral edema model in *ex vivo* rat brain slice preparations

Brain slice preparation, incubation media and experimental protocols. Adult male Wistar rats (body weight: 250 g; n = 47) were decapitated under deep anesthesia (4–5% isoflurane in $N_2O:O_2$; 2:1), and coronal brain slices were prepared as reported previously and given as supplement to the paper.[25]

Hypo-osmotic solutions were prepared by reducing the NaCl concentration of aCSF from the regular 130 to 40-120 mM (HM_{40}–HM_{120}), while other components and the pH of the medium were unaltered. The results shown in this paper were obtained with HM_{100} and HM_{60}. The use of HM_{60} was relevant for the pharmacological set of experiments, because this condition regularly evoked spontaneous SDs to be modified by the

drugs used. Hyper-osmotic solutions (HRM) contained additional mannitol in normal aCSF at 100 mM concentration (n = 11). Over the experimental protocol, control slices were incubated in aCSF throughout the recording (n = 21), whereas aCSF was replaced with HM (i.e. typically HM_{100} or HM_{60}) in the recording chamber as the experimental condition (n = 57, HM_{100}: 16 slices, HM_{60}: 41 slices).

In control slices incubated in aCSF, SD1 was triggered by electric stimulation as reported earlier.[30] A subsequent, recurrent SD (rSD) was elicited by transient anoxia (i.e. the replacement of O_2 with N_2 in the gas mixture applied to bubble the aCSF for 2.5 min). Under HM, SD1 typically occurred spontaneously in response to osmotic stress, and the subsequent event was elicited 15 min later with transient anoxia.

To characterize the excitability of the nervous tissue, evoked field potentials (EFP) were recorded from layer 3-4 of the somatosensory cortex, or CA1 region of the hippocampus. Slices were incubated in aCSF or in HM. Stimulation was delivered by a concentric bipolar needle electrode. The distance between the current delivery electrode and recording microelectrode was approximately 800 μm. Stimulation was implemented with single constant current pulses (5–15 μA, 1 ms).

LFP recordings. LFP measurements filtered in DC mode (<1Hz) were acquired via two glass capillary microelectrodes (1–3 MΩ) filled with 150 mM NaCl and 1 mM HEPES, inserted into the 3rd cortical layer at a distance of 1000 μm. An Ag/AgCl electrode was placed in the recording chamber and served as reference (see Supplementary material).[25]

Intrinsic optical signal imaging. For IOS imaging, slices were illuminated by a halogen lamp (Volpi AG, Intralux 5100, Schlieren, Switzerland). Image sequences were captured at 1 Hz with a monochrome CCD camera (spatial resolution: 1024 × 1024 pixel, Pantera 1M30, DALSA, Gröbenzell, Germany) attached to a stereomicroscope (MZ12.5, Leica Microsystems, Wetzlar, Germany), yielding 6–10× magnification. Changes in IOS intensity were extracted at three ROIs positioned along the propagation of SD1, and expressed relative to baseline intensity (ΔI/I). Image sequences were used off line to measure the degree of slice swelling associated with osmotic stress or depolarization events.

Pharmacological treatments. Slices were randomly exposed to various pharmacological treatments: (i) For edema reduction, Na^+/K^+/Cl^- cotransporter blocker Bumetanide (Bum, Sigma-Aldrich; 1 mM) and the aquaporin-4 channel inhibitor TGN-020 (Tocris; 100 μM) were co-applied (n = 16) (ii) to inhibit

swelling related glutamate efflux via volume-regulated anion channels (VRAC), slices were exposed to the channel blocker DCPIB (Tocris; $20\,\mu M$) ($n = 21$); (iii) N-methyl D-aspartate (NMDA) receptors were blocked by the non-competitive NMDA receptor antagonist MK-801 (Tocris; $100\,\mu M$), co-applied with the competitive α-amino-3-hydroxy-5-methyl-4-isoxazolepropionic acid AMPA/kainate receptor antagonist CNQX (Tocris; $20\,\mu M$) ($n = 13$); (iv) TFB-TBOA (Tocris; $10\,\mu M$ and $100\,\mu M$) an excitatory amino acid transporter inhibitor was washed on the slices to explore whether glutamate uptake was functional ($n = 4$); (v) Finally, fluorocitrate (Sigma; 0.5–1 mM), a drug that disrupts the citrate cycle in astrocytes was applied to paralyze astrocytes ($n = 7$) (see Supplementary Material for solution).[31–35] In case no spontaneous SD1 occurred, the slices were not considered for further analysis.

To evaluate the impact of HRM on the assessed variables, slices were incubated in HM first (i.e. typically HM_{100} or HM_{60}) for 30 min, then HM was replaced with HRM. The first SD (SD1) occurred spontaneously in HM. A subsequent, recurrent SD (rSD) was elicited by transient anoxia in HRM.

Histology. The size of the ischemic lesion was determined by triphenyltetrazolium chloride (TTC) staining. To examine the morphology and swelling of astrocytes, a modified Golgi-Cox staining was used.[36] Cross cortical blocks were dissected from representative brain slices for electron microscopic examination (see Supplementary material).

Statistical analysis

Data analysis was conducted offline and was assisted by the inbuilt tools of dedicated software (AcqKnowledge 4.2 for MP 150, Biopac Systems, Inc., USA and eDAQ Chart, eDAQ Pty Ltd., Colorado Springs, CO, USA). Blinding data analysis was intended by assigning codes to files and recordings, which do not reveal the experimental condition (i.e., date of the experiment). The exact steps of analysis are given in the Supplementary material. Image processing was performed after background subtraction and thresholding in Fiji detailed in the Supplementary material.

Quantitative data are given as mean ± standard deviation (stdev). Statistical analysis was conducted with the software SPSS (IBM SPSS Statistics for Windows, Version 22.0, IBM Corp.). Data sets were evaluated first with a Shapiro-Wilk test of normality. For data with normal distribution, an independent samples T-test, a one-way analysis of variance (ANOVA), a two-way ANOVA or repeated measures were used, followed by a Sidak post hoc test when appropriate. Non-parametric data were evaluated with a Kruskall Wallis test, followed by a Tukey's or a Dunn's post hoc analysis. Levels of significance were set at $p < 0.05^*$ or $p < 0.01^{**}$. Distinct statistical methods are provided in each Figure legend in detail.

Data availability

The datasets generated during and/or analyzed during the current study are available from the corresponding author on reasonable request.

Results

Simultaneous depolarization is linked to acute tissue swelling in the rat cerebral cortex

The physiological variables are given in the Supplementary Material (Suppl. Table 1). In the rat 2VO model, the first SD (SD1) evolved in response to ischemia induction (propagation velocity: 2.91 ± 1.18 mm/min), when the basal CBF decreased to $23.6 \pm 5.9\%$ of baseline (Suppl. Figure 1). Approximately 50 minutes later, an SiD occurred (i.e. a depolarization event observed simultaneously at the two electrodes 4.5 mm apart) after anoxia induction, in the cortical area previously invaded by SD1 ($n = 5$) (Figure 1(B_2) and Suppl. Figure 1). In other rats ($n = 6$), a propagating SD (recurrent SD, rSD; rate: 5.66 ± 1.23 mm/min) emerged upon anoxia (Figure 1(B_1)). SiD was preceded by local CBF values lower than before rSDs (20.2 ± 2.5 vs. $45.6 \pm 9.6\%$; for SiD vs. rSD) (Figure 1(c)). The low CBF prior to SiD could have been linked to the physical compression of microvessels due to the space occupying swelling of the nervous tissue, which probably overrides endothelium-based CBF regulation.[37]

SiD was also confirmed after KCl evoked SDs in a rat ischemia/reperfusion model. The IOS intensity increase typical of SD was simultaneous after terminal anoxia ($n = 7$; Figure 1(D_2), ROI2-4; Suppl. video 1). This bulk of tissue was identified as an extensive SD focus (4.62 ± 0.95 mm^2), from which the depolarization spread (Figure 1(D_2), ROI1; rate: 4.5 mm/min). In contrast, prior KCl evoked SDs originated from a punctual focus (0.95 ± 0.51 mm^2) (Figure 1(D_1) and (E)) and spread over the full field of view (rate: 3.5 ± 0.8 mm/min) (Suppl. Video 2). SiD was recognized as the pathological expansion of the focal region of SD.

Coincidentally, acute tissue swelling was observed in response to anoxia, shortly before SiD occurrence (Suppl. Video 3). Edema progression was obvious before SiD, but negligible with ischemia- or KCl-evoked SDs (Figure 1(f) and (g)). Accordingly, we hypothesized that acute tissue swelling may drive the
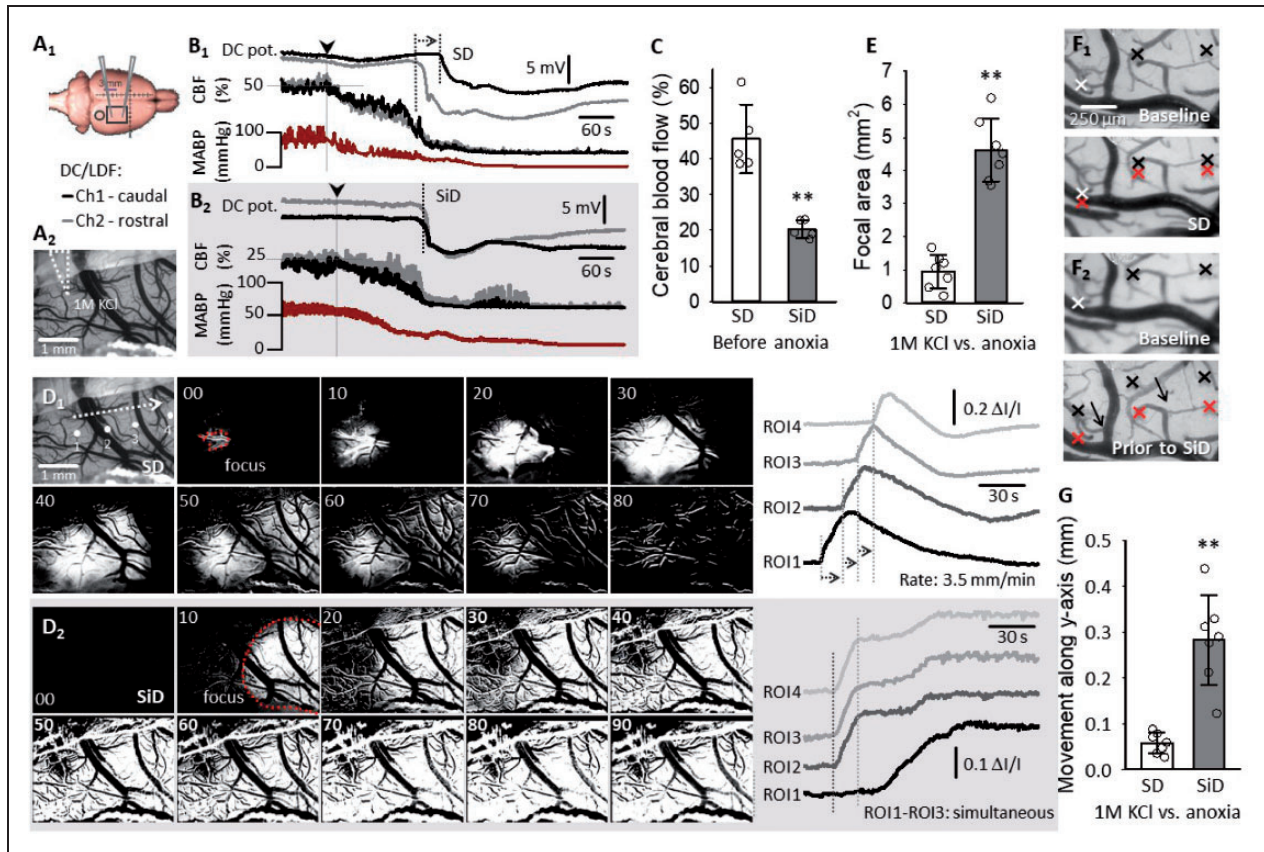
Figure 1. The evolution of simultaneous depolarization (SiD) upon anoxia induction is linked to acute tissue swelling. (a) Illustration of electrode positions in the rat cerebral cortex (A_1). A representative image of a cranial window incorporating a capillary for SD elicitation with 1 μl KCl (A_2) (b) Anoxia-triggered spreading depolarization (recurrent, SD, rSD; 6 of 11 rats) (B_1), or SiD (5 of 11 rats) (B_2) in the hypoperfused cortex (i.e. 2VO model). (c) CBF levels before anoxia initiation, relative to baseline taken prior to ischemia induction. (d) Background subtracted intrinsic optical signal (IOS) image sequences show SD propagation from a confined focus at the site of elicitation with 1 M KCl (D_1). Traces derived from four regions of interest (ROIs) confirm the propagation of the SD. In contrast, anoxia triggered SiD that appeared at ROI2, ROI3 and ROI4 in synchrony, and involved a considerable part of field of view simultaneously (D_2). The time elapsed (s) with respect to the first image is shown in the upper left corner in each image. (e) The size of the SD/SiD focal area. (f) Acute tissue swelling is shown with the shift of contrast edge markers on IOS images. Note the position of the red markers with SD (F_1) and prior to SiD (F_2) with respect to the black markers placed prior to KCl ejection or anoxia. (g) Quantification of tissue swelling during SD and SiD. Data in (c, e and g) are given as mean ± stdev, individual values are shown with a dot plot. The distribution of data was evaluated by a Shapiro-Wilk test of normality (c, $p = 0.063$; e, $p = 0.902$; g, $p = 0.112$), which was followed by a paired sample T test ($p < 0.05*p < 0.01**$). CBF: cerebral blood flow; MABP: mean arterial blood pressure.

expansion of the SD focus. To explore this concept, we moved on to experiment on *ex vivo* brain slice preparations, which offered the controlled induction of tissue edema, and the reliable visualization of the SD focus.

Hypo-osmotic stress favors the evolution of SiD

To test the hypothesis that acute tissue swelling expands SD focus, we created extreme hypo-osmotic stress in *ex vivo* brain slice preparations. SD1 occurred spontaneously during HM incubation or was elicited by electrical stimulation in normal aCSF (Figure 2). Anoxia caused propagating rSD under aCSF (Figure 2(a)) but induced SiD predominantly in HM (35 of 44 slices, 80%)

(Figure 2(b) and (d)). In a few cases (n = 3), SiD in HM was spontaneous, before anoxia (Suppl. Figure 2 (a)). Repolarization after SD1 in HM was substantially delayed or incomplete, and small amplitude, irregular field oscillations evolved in synchrony on the DC potential trace (Figure 2(b); Suppl. Figure 2(b)). These field oscillations predicted the later SiD.

The IOS signature of SDs was validated in a few slices, by the synchronous recording of the DC potential (Suppl. Figure 3). The focus of SD1 was punctual (<1% of total cortical area) in both aCSF and HM, and was localized to the upper layers of the dorsal-dorsolateral parietal cortex (Figure 2(c) and (e)). SD1 propagated with a higher rate in HM than in aCSF (3.17 ± 0.58
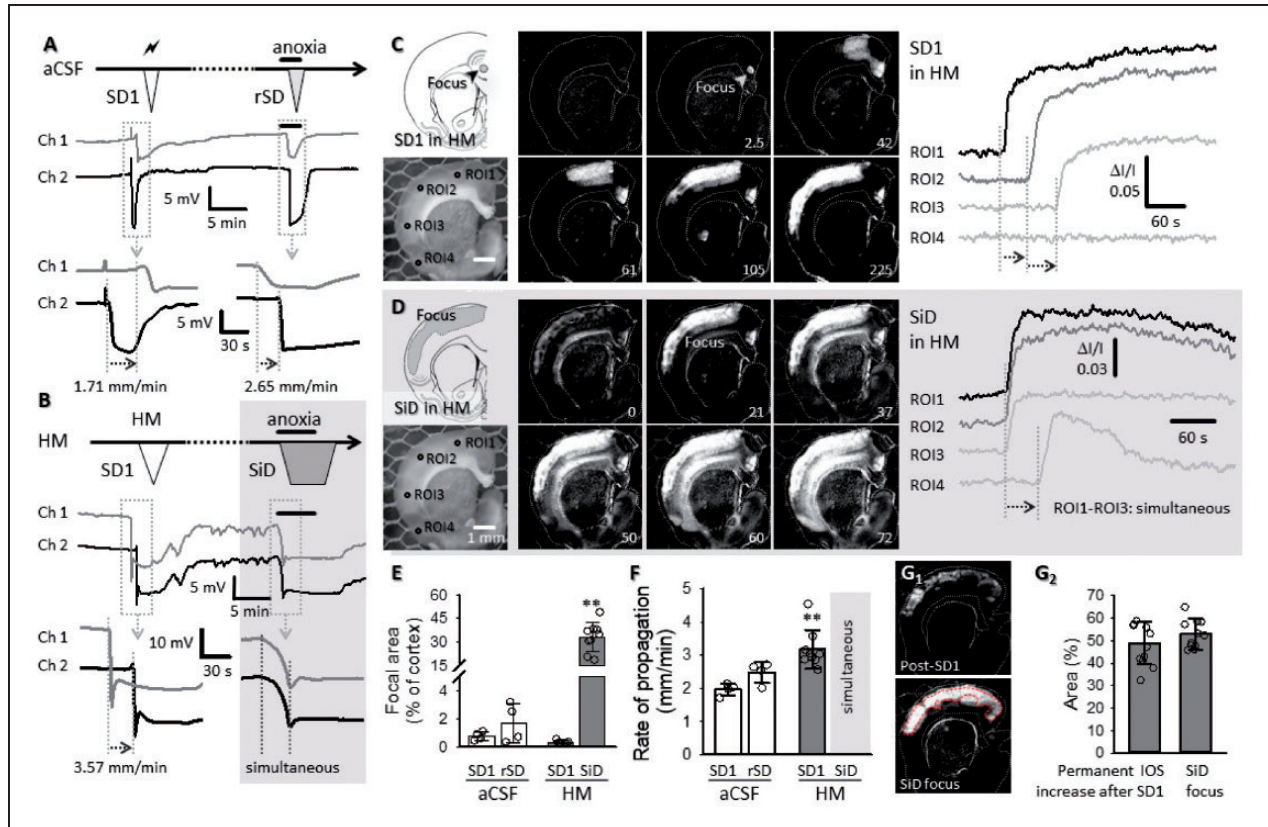
Figure 2. Replication of SD and SiD during osmotic stress in rat *ex vivo* coronal brain slice preparations. (a) The regular spreading nature of both SD1 and rSD in normal aCSF is shown in a representative electrophysiology experiment. SD1 was elicited by electrical stimulation and rSD was induced by transient anoxia (oxygen withdrawal of 2.5. min). (b) SD1 occurred spontaneously to HM exposure (HM_{60} here), while the subsequent event was induced 15 min later by transient anoxia. The original electrophysiological recordings demonstrate that SD1 was a spreading event, followed by an SiD in response to anoxia. (c and d) In background subtracted IOS images of a HM-incubated brain slice, the temporal characteristics of SD1 (c) reveal a punctual focus and propagation in the upper cortical layers. (d) Subsequent anoxia in HM (HM_{100} here) induced SiD of an extensive bulk of cortical tissue (ROI1-ROI3; SiD), and the propagation of the event towards the ventral tips of the cortex (ROI3 → ROI4). Note the simultaneous increase of signal intensity (Panel D) at ROI1-ROI3, and the delay at ROI4 with respect to ROI1. (e) The relative size of the focal area of SD/SiD measured in IOS images. (f) The focal area of SiD incorporated the tissue zone characterized by sustained IOS intensity elevation following SD1. Images in F_1 were taken prior to SiD (post-SD1), and at the emergence of SiD (SiD focus). A red broken line delineates the post-SD1 high IOS intensity zone (the later SiD focus). The mean size of the tissue area is given in F_2 relative to the full size of the cortex. (g) The rate of propagation of depolarization events. (e to g) Data are given as mean ± stdev, individual values are shown with a dot plot. A Shapiro-Wilk test of normality indicated normal non-normal distribution for (e and f) (p = 0.050*), and normal distribution for Panel G_2 (p = 0.304). Accordingly, data in (e and f) were analyzed with a non-parametric Kruskal-Wallis test, followed by a Dunn post hoc analysis (E, p < 0.01** vs. SD1 in HM; F, p < 0.01** vs. SD1 in aCSF). Data in (G_2) were evaluated with a one-way ANOVA paradigm, followed by a Sidak post hoc test whenever relevant (p < 0.05*p < 0.01**).

vs. 1.97 ± 0.18 mm/min, HM vs. aCSF) (Figure 2(f)). Anoxia in HM gave rise to SiD in 11 of 16 slices, implicating a sizeable area of the cortex (>50% of the total cortical area), which incorporated much of the tissue previously involved in SD1 propagation (Figure 2(d) and (g)). In addition to the upper cortex, SiD progressively engaged the underlying deeper layer of the cortex (Figure 2(d)). Also, SD took off at the ventral edge of the SiD (Figure 2(d)). In 5 of 16 slices, spatially distinct, multifocal SDs occurred upon anoxia (Suppl. Figure 3 (b)). Multifocal rSD was considered as a transition between classic rSD (i.e. single focus) and SiD.

Collectively, these data show that under osmotic stress, the tissue engaged in the propagation of SD1 later turned into a sizeable depolarization focus identified as SiD. The elevated IOS intensity sustained after SD1 (Figure 2(G_1)) and the concomitant failure of complete repolarization from SD1 (Suppl. Figure 3(a)) together predicted SiD occurrence.

Astrocyte swelling is implicated in SiD

To further explore the hypothesis that tissue swelling predisposes the tissue to SiD, we evaluated the degree

of tissue swelling caused by the osmotic stress. The increase of the brain slice area was most conspicuous with the second depolarization event, rSD in aCSF and SiD in HM (Figure 3(A_{1-2})). Under aCSF, slice surface area increased slightly with SD1 (with $1.09 \pm 0.68\%$) and returned to baseline within minutes after SD1 ($0.19 \pm 0.15\%$). The maximum increase of slice area was greater with rSD than with SD1 (4.75 ± 1.33 vs. $1.09 \pm 0.68\%$, rSD vs. SD1), but the swelling was again transient and reversible (Figure 3(A_3) and Suppl. Figure 4). In HM, slice swelling commenced upon HM exposure, and the slice area gradually increased to reach a considerable expansion already before SD1 (4.59 ± 1.14 and 4.15 ± 1.11 vs. $0.07 \pm 0.09\%$, HM_{60} and HM_{100} vs. aCSF) (Figure 3(A_4)

and Suppl. Figure 4). SD1 in HM occurred then spontaneously, and increased slice area with an additional, small extent (6.9 ± 2.6 and $5.94 \pm 2\%$ HM_{60} and HM_{100}). The slice area showed negligible variations afterwards, with no recovery to pre-SD1 level (Figure 3(A_4) and Suppl. Figure 4). It is important that slice swelling preceded SD1 and SiD in HM, in contrast with aCSF, in which slice swelling was associated with SD1 and rSD.

Next, since astrocytes rapidly swell in response to hypo-osmotic stress we hypothesized the pivotal role of astroglial edema in our HM model.[38] Astrocytes appeared clearly swollen in Golgi-Cox-stained slices and electron microscopic preparations after exposure to the hypo-osmotic medium, especially after the
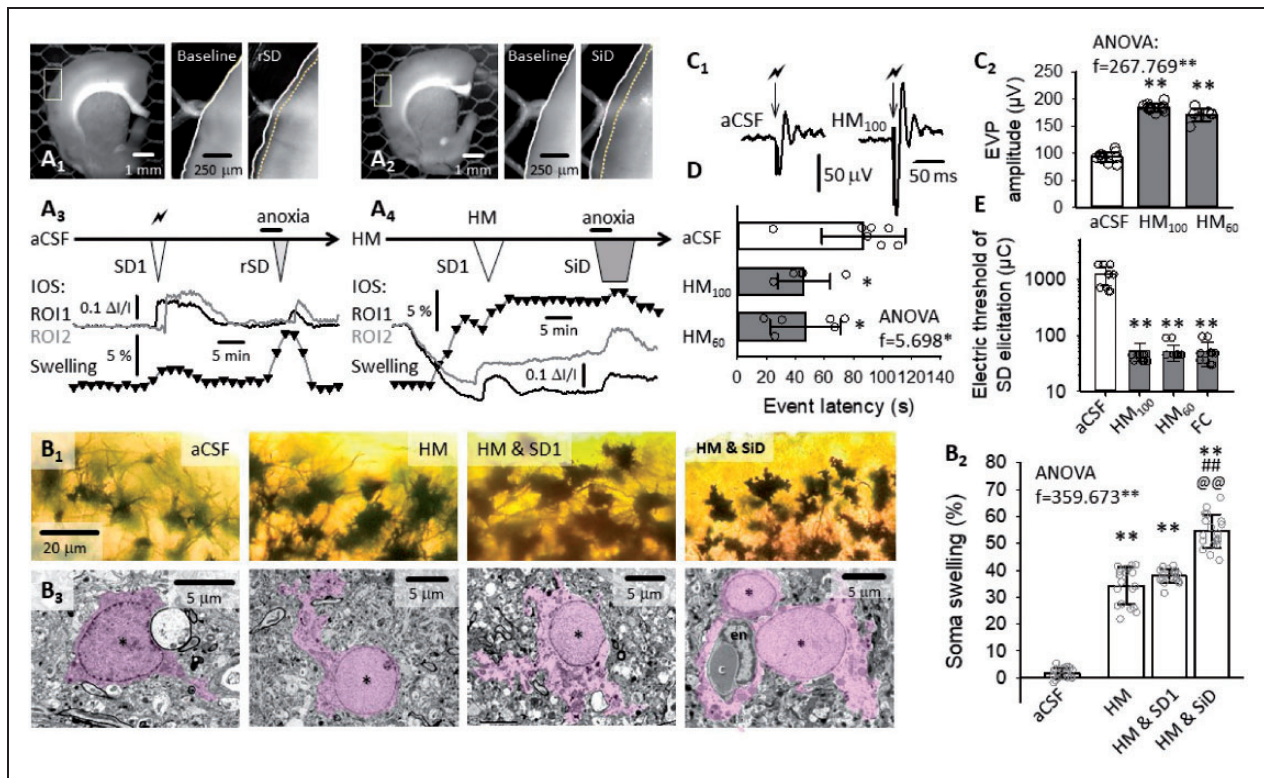

Figure 3. The implication of tissue edema and astrocyte swelling in SiD evolution in brain slices. (a) IOS images demonstrate slice swelling with rSD in normal aCSF (A_1), and with SiD in HM (A_2), represented by the displacement of the contour of the parieto-temporal cortex (inserts). Swelling over the experimental protocol was characterized by the change in the surface area of the full slice relative to baseline, at a temporal resolution of 1/100 s (trace with black triangles), and depicted in temporal correspondence with IOS variations at two ROIs (aCSF: A_3; HM: A_4). (b) Golgi-Cox-stained sections (B_1) and electron photomicrographs (B_2) of astrocytes in aCSF, HM after SD1 in HM and after SiD in HM (asterisk: astrocyte nucleus; purple shading astrocyte plasma and nucleus, c: capillary lumen filled with an erythrocyte). The soma swelling of astrocytes was measured in Golgi-Cox-stained preparations, and have been expressed relative to soma size in aCSF (B_3). (c) The excitability of the nervous tissue. The amplitude of evoked field potentials (EFP) was twice as great in HM compared to aCSF, as shown in representative recordings (C_1) and a quantitative bar chart (C_2). (d) Latency of rSD in aCSF and SiD in HM after anoxia. (e) The electric threshold of SD elicitation under aCSF, HM or fluorocitrate (FC) incubation. Data in Panels (B_3, C_2, d and e) are given as mean $\pm$ stdev. Dot plots depict individual values in (B_3, C_2, and d). Normal distribution of data was confirmed by a Shapiro-Wilk test (B_3, $p = 0.675$; C_2, $p = 0.585$; D, $p = 0.146$; e, $p = 0.05*$). Further statistical analysis was achieved with a one-way ANOVA ($p < 0.05*$ and $p < 0.01**$), and a Sidak post hoc test ($p < 0.05*$ and $p < 0.01**$ vs. aCSF; in B_3, $p < 0.01^{\#\#}$ vs. HM, $p < 0.01^{@@}$ vs. HM & SD1), or a Kruskal Wallis test followed by a Dunn's post hoc test (e, $p < 0.01**$ vs. aCSF).

passage of SD1 (Figure 3(B$_1$)), substantiated by the quantitative evaluation of astrocyte soma area in the Golgi-Cox-stained section (Figure 3(B$_2$)). In the electron microscopic images, both the perinuclear plasma and astrocyte processes appear to increase in size. The astrocyte plasma displayed decreased electron density indicative of cellular edema, particularly after SD1 had been superimposed to the osmotic stress (Figure 3(B$_3$)).

Consequently, we posited further that swollen astrocytes must substantially contribute to SiD, because astrocyte swelling increases neuronal excitability.[10] EFP amplitude measured in the cerebral cortex was significantly greater in HM (171.0 ± 11.8 and 184.3 ± 7.4 vs. $93.1 \pm 9.3 \mu V$, HM$_{60}$ and HM$_{100}$ vs. aCSF) (Figure 3(c)). The latency of SiD occurrence to anoxia onset decreased markedly in HM (46.9 ± 24.3 and 45.9 ± 18.2 vs. 86.9 ± 28.7 s; SiD in HM$_{60}$ and HM$_{100}$ vs. rSD in aCSF) (Figure 3(d)). Likewise, the electric threshold of SD elicitation was drastically reduced in HM (50.1 ± 15.7 and 52.5 ± 18.4 vs. $1214.3 \pm 470.6 \mu C$, HM$_{60}$ and HM$_{100}$ vs. aCSF) (Figure 3(e)). In the latter set of experiments, the implication of astrocyte swelling was confirmed by repeating the SD threshold measurements with the addition of fluorocitrate to the aCSF, which decreased SD threshold similar to HM (51.0 ± 22.9 and $52.5 \pm 18.4 \mu C$, fluorocitrate and HM$_{100}$) (Figure 3(e)).

SiD evolution promotes lesion maturation

SD has been proposed to recruit viable ischemic penumbra tissue into the infarcted core.[3] Further, persistent cytotoxic edema has been implicated in the SD related dendritic injury.[17] Given this context, we hypothesized that astroglial swelling and the related SiD must have represented the actual tissue infarction in progress. We observed that the maximum depolarized tissue area engaged in SiD was invariably greater than the tissue area traversed by SD1 (76.8 ± 11.4 vs. $60.9 \pm 10.7\%$, SiD vs. SD1) (Figure 4(a) and (c)). Macroscopic tissue
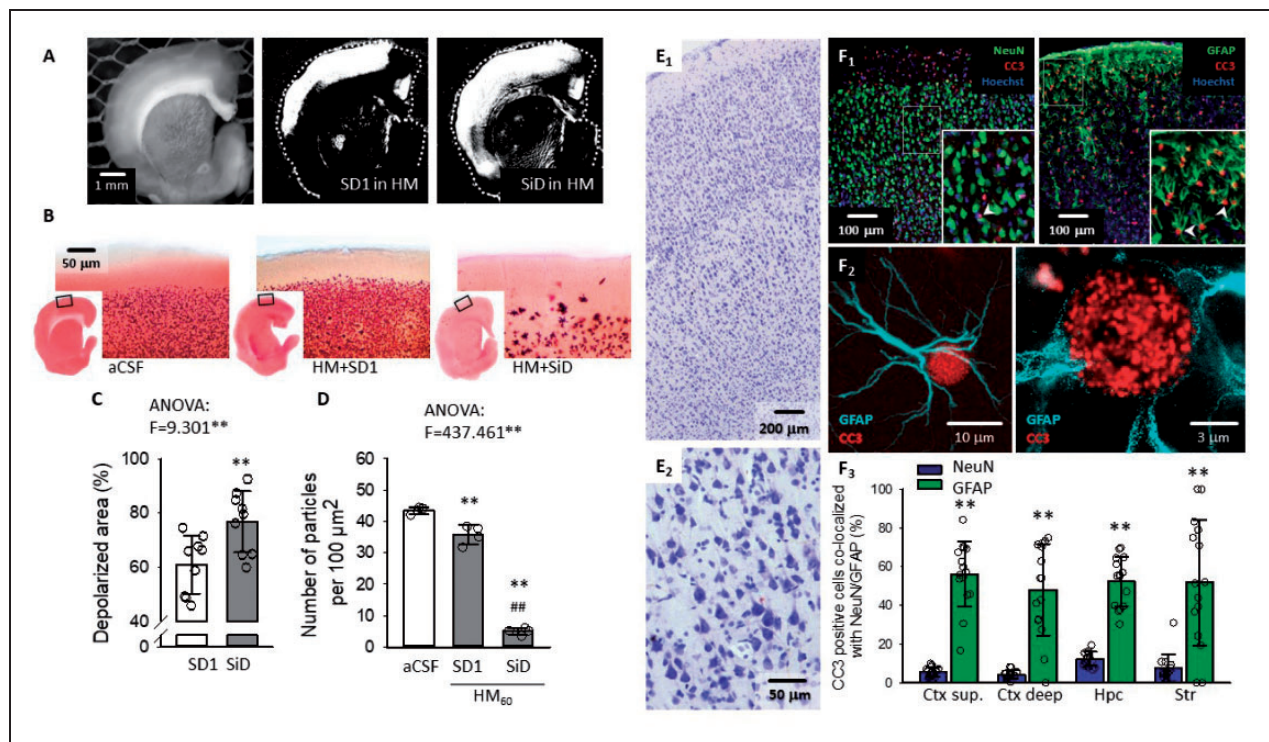

Figure 4. Cellular injury as a consequence of SD or SiD. (a) The area covered by SD1 and the subsequent SiD as shown in representative background subtracted IOS images. (b) TTC staining of brain slices after SD1 in aCSF, HM, and SiD in HM. (c) Quantitative evaluation of the total area covered by SD1 and SiD. (d) The number of TTC-stained cellular compartments (i.e. particles) after depolarization events. (e) Pyramidal cell necrosis after SiD, visualized in the parietal cortex of anesthetized rats with Nissl staining. (f) Immunocytochemical co-localization of cleaved caspase-3 (CC3) with cell nuclei (Hoechst) of neurons (NeuN) and astrocytes (GFAP) shows predominant glial apoptosis after SiD (F$_1$). Super-resolution (STED) microscopy unravels the nuclear localization of CC3. Quantitative analysis of astrocyte apoptosis in the cerebral cortex (Ctx), hippocampus (Hpc) and striatum (Str) (F$_3$). Data in (c, d and F$_3$) are given as mean $\pm$ stdev; additional dot plots show individual values. After the evaluation of normal distribution with a Shapiro-Wilk test (c, p = 0.077; d, p = 0.616; F$_3$, p = 0.050*), statistical analysis relied on a one-way ANOVA in Panels C & D, p < 0.01**, followed by a Sidak post hoc test (c: p < 0.01** vs. SD1; d: p < 0.01** vs. aCSF, p < 0.01### vs. SD1 in HM). In Panel F$_3$, a non-parametric Kruskal-Wallis test was used, followed by a Tukey post hoc test (p < 0.01** vs. NeuN).

damage assessed with TTC staining was obvious after SiD compared to SD1 in HM, or aCSF (Figure 4(b)). The number of TTC-positive cellular compartments (i.e. "particles") was clearly reduced after SiD compared to SD1 in HM or aCSF (5.0 ± 1.1 vs. 35.8 ± 3.0 vs. 43.5 ± 1.0 particles per 1000 μm^2, SiD in HM vs. SD1 in HM vs. aCSF) (Figure 4(d)).

Complementary results were obtained from the ischemic/anoxic brains of anesthetized rats. Twenty-five minutes after SiD occurrence, conventional Nissl-staining disclosed widespread neuronal necrosis in the cortex (Figure 4(e)). At the same time, the immunocytochemical co-localization of cleaved caspase-3 (CC3) with NeuN or GFAP identified predominant astrocyte apoptosis (Figure 4(f)). Approximately 50% of all GFAP-labeled astrocytes were CC3 positive in the parietal cortex, hippocampus and striatum, whereas only 4-12% of NeuN-labeled neurons expressed CC3 (Figure 4(F_3)).

Our histological results together suggest that astrocytic edema and the linked SiD seriously jeopardize the survival of neurons and astrocytes alike and impose significant damage to the nervous tissue.

Inhibition of astrocyte swelling or volume regulated glutamate release alleviates tissue edema and prevents SiD

Next, we set out to understand the underlying mechanisms of SiD by attempting to prevent it by pharmacological means. Edema-related glutamate release or impaired glutamate clearance emerged as the most likely candidates to promote SiD, because astrocytes have been shown to swell and release glutamate in response to osmotic stress and spreading depolarization.[39–41] To test this notion, extracellular glutamate concentration concomitant with slice swelling in HM was characterized.

Extracellular glutamate gradually accumulated with slice swelling, to exceed $10 \mu M$ concentration by the time SD1 occurred. SD1 was associated with a glutamate peak followed by partially recovery. Then extracellular glutamate concentration remained constantly elevated above $15 \mu M$, coincident with ongoing slice swelling. SiD caused a second glutamate peak with no recovery ($>20 \mu M$) against a background of marked edema (Figure 5(a) and (C_2)). Similarly, the extensive extracellular glutamate accumulation after SD1 was followed by SiD in the anesthetized rat (Figure 5(C_1)).

Inhibition of astrocyte AQP4 channels and $Na^+/K^+/Cl^-$ co-transporters (NKCCs) by TGN-020 + Bumetanide (TGN + Bum), or volume regulated anion channels (VRACs) by DCPIB effectively reduced slice swelling related to HM exposure and SD (Figure 5

(b)). Furthermore, TGN+Bum or DCPIB profoundly diminished extracellular glutamate accumulation with SD1, and improved the glutamate recovery after anoxia (Figure 5(C_2) and (d)). Furthermore, both treatments decreased the likelihood of SiD evolution significantly (2 of 16 (13%) vs. 3 of 23 (13%) vs. 28 of 33 (85%) slices; TGM+Bum vs. DCPIB vs. HM_{60}). Instead, the majority of the treated slices gave rise to rSD in response to anoxia. This was reflected in the size of the focal area of depolarization events. While the SD1 focus was punctual and very small (<1% of the cortical surface) in all groups (Figure 5(e)), the focus of SiD in the HM_{60} group engaged $55.5 \pm 7.2\%$ of the cortex. In contrast, the rSD focus in the TGN+Bum and DCPIB groups was much more confined (Figure 5(e)). Taken together, the inhibition of astrocyte swelling by TGN-020 + Bumetanide or DCPIB evidently blocked SiD evolution.

Next, we asked whether astrocyte dysfunction is sufficient to produce the SiD phenotype in normal aCSF. Fluorocitrate treatment to arrest astrocyte metabolism replicated slice pathology in HM; (i) The SD elicitation threshold decreased (Figure 3(e)); (ii) SD1 emerged spontaneously (4 of 5 slices), and (iii) SiD evolved upon subsequent anoxia (3 of 5 slices) (Figure 5(f)). In line with these data, inhibition of astrocyte glutamate transporter-2 (EAAT2) caused profound extracellular glutamate accumulation to $29.5 \pm 9.9 \mu M$, which was followed by the spontaneous occurrence of an SiD (3 of 4 slices) (Figure 5(g)). Extracellular glutamate accumulation with SiD peaked at $65.3 \pm 18.1 \mu M$, followed by further extracellular glutamate accumulation without any recovery. These data further substantiated that extracellular glutamate accumulation (due to intensified release or impaired uptake by swollen astroglia) must have mediated SiD in HM.

The blockade of neuronal NMDA+AMPA receptors (CNQX+MK801) was ineffective against slice swelling in HM (Suppl. Figure 5). Furthermore, glutamate receptor antagonists were the least effective against extracellular glutamate accumulation. Under CNQX+MK801 incubation, multifocal rSDs occurred, as seen in a few HM slices before (Suppl. Figure 3(b)). These observations confirmed the pivotal role of astrocytes in tissue swelling and the related impaired glutamate clearance.

Hyperosmotic treatment reverses tissue swelling, restores physiological extracellular glutamate concentration, and prevents SiD

Taken the results above, we hypothesized that the complete reversal of cellular edema by hyperosmotic treatment could restore extracellular glutamate levels to the physiological range, and prevent SiD. To test this
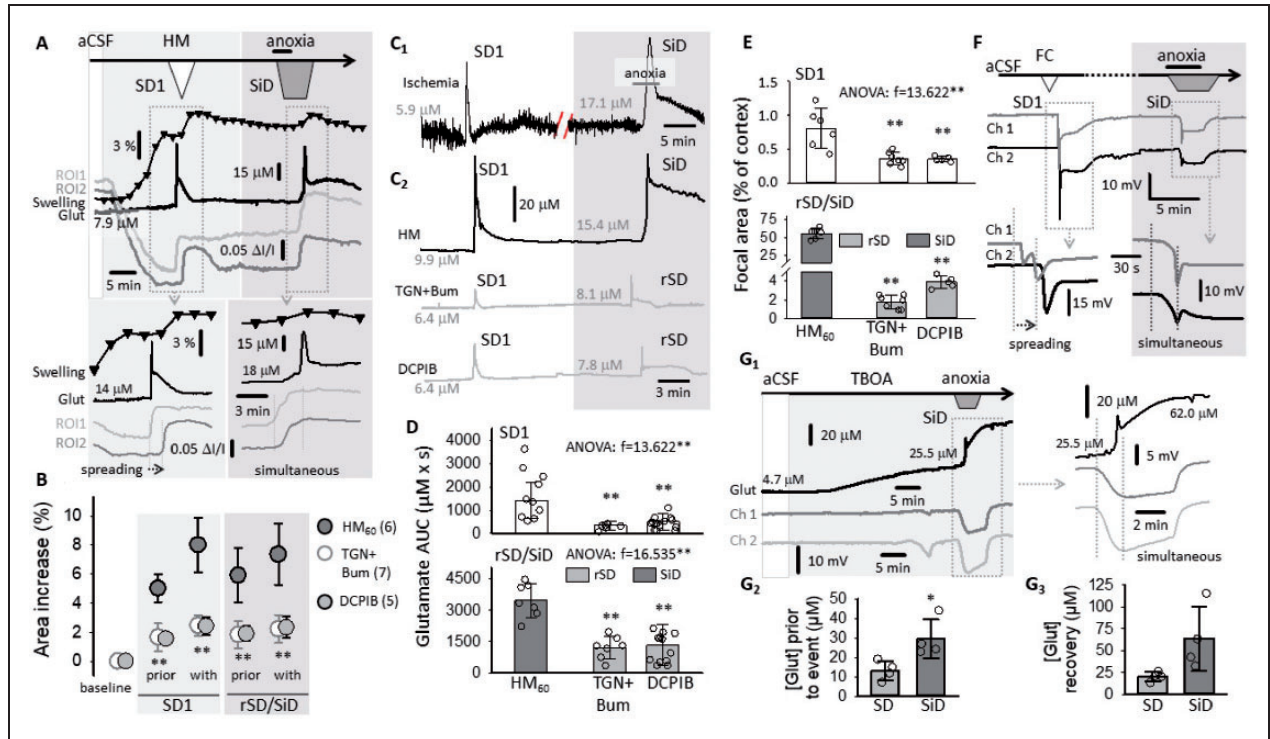
Figure 5. Inhibition of glial swelling or volume regulated glutamate release attenuates SiD. (a) Spatiotemporal relationship between tissue swelling (black trace with black triangles), depolarization events (IOS intensity changes at ROI1 and ROI2, gray traces), and changes in glutamate concentration (black trace) in brain slices. (b) The impact of pharmacological treatments on slice swelling relative to baseline at selected time points. (c) Representative extracellular glutamate concentration traces during SD and SiD in the cortex of an anesthetized rat (C_1) and in ex vivo brain slice preparations (C_2). (d) The accumulation of glutamate with SD1 and rSD/SiD (area under the curve, AUC). (e) The impact of pharmacological treatments on the size of the focal area of SD1 and rSD/SiD relative to the area of the cortex. (f) The application of fluorocitrate (FC) to brain slices replicated the SiD phenotype is aCSF. (g) Representative recordings of glutamate concentration (Glut) and DC potential (Ch1 and Ch2) under TBOA treatment – note the occurrence of SiD (G_1), and high glutamate concentration at two selected phases of these experiments (G_{2-3}). Data in (b, d, e and G_{2-3}) are given as mean±stdev. Dot plots in (d, e and G_{2-3}) show individual values. Statistical analysis was conducted with a Shapiro-Wilk normality test (b, p = 0.255; d, p = 0.110; e, p = 0,050*; G_2, p = 0.158; G_3, p = 0.127), and a repeated measures model (b: F_{time}=196.228**; F_{treat}=29.805**) or one-way ANOVA (D, G_{2-3}; p < 0.01**) or a Kruskal-Wallis test (E, p < 0.01**) followed by a Sidak or a Dunn's post hoc test (b, d, e: p < 0.01** vs. HM_{60}; G: p < 0.05* vs. SD).

hypothesis, HM was substituted with a hyperosmotic medium (HRM) after 30 min HM incubation, and the slice was challenged with anoxia as above. HRM completely reversed slice swelling, restored physiological extracellular glutamate concentration, and promoted the recovery of the IOS signal (Figure 6(a), center). Further, HRM exposure completely prevented the occurrence of any depolarization and extracellular glutamate accumulation upon anoxia (Figure 6(a), right). The electrical threshold of SD elicitation was also markedly increased under HRM (2422.5 ± 341.7 vs. 54.0 ± 2.1 vs. 1220.0 ± 6.2 µC, HRM vs. HM_{100} vs. aCSF) (Figure 6(b)). The coincidence between slice swelling and extracellular glutamate concentration was further supported by their strong positive linear correlation (r = 0.819**) (Figure 6(c)). We concluded that extracellular glutamate content was tightly coupled to tissue edema, and that anti-edema treatment

effectively counteracted extracellular glutamate accumulation and SiD.

Recapitulation of astrocyte swelling and SiD in the in vivo water intoxication model of cytotoxic edema

Next, we revisited our original assumption that edema is the precondition for SiD, and tested the hypothesis in the water intoxication model of cytotoxic edema in rats (Figure 6(d)). SD1 was elicited experimentally with KCl and was followed by a terminal SiD upon anoxia in 6 of 7 rats. In the control condition (saline i.p.), anoxia induced a classic SD in 4 of 4 rats. The KCl-induced SDs superimposed on cerebral edema lasted considerably longer than similar SDs in control rats (94.4 ± 48.3 vs. 30.4 ± 11.1 s, water intoxication vs. saline) (Figure 6(h)), which stood in agreement with the
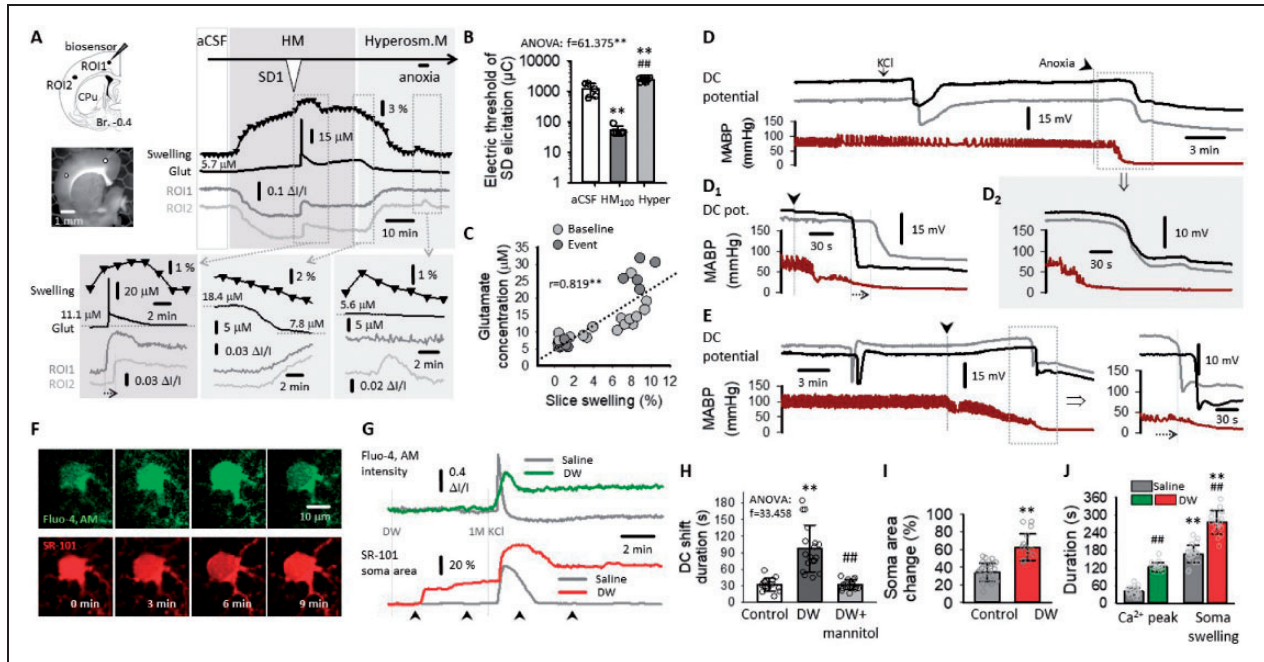
Figure 6. Reversal of slice swelling and SiD to SD with hyperosmotic medium (HRM). (a) Changes of glutamate (Glut) accumulation and IOS signal (ROI1 & ROI2) after HRM treatment. (b) The impact of HRM on the electrical threshold of SD elicitation, with respect to aCSF and HM_{100}. (c) Correlation between glutamate concentration and slice swelling. (d) Representative DC potential traces (at two microelectrodes 3 mm apart) and mean arterial blood pressure – (MABP) after intraperitoneal (i.p.) injection of distilled water (DW). A spreading depolarization (SD) occurred upon anoxia (black arrowhead) in the control condition (the i.p. injection of physiological saline) (D_1). Simultaneous depolarization (SiD) triggered with anoxia was recorded after water intoxication with i.p. DW injection (D_2). (e) A propagating SD emerged upon anoxia (black arrowhead) after the administration of mannitol (i.v.) in the water intoxication model (i.p. DW). (f) Two-photon imaging of intracellular calcium waves (Fluo-4, AM) in astrocytes, and astrocyte soma volume (SR-101) in the cerebral cortex of anesthetized mice. (g) Representative traces derived from the experiment presented in Panel E show the intracellular accumulation of Ca^{2+} and astrocyte soma swelling with SD after water intoxication (DW) with respect to control (saline). Arrowheads beneath the traces show the time instant of the images in Panel (e). (h) The duration of the DC shift with SDs in anesthetized rats. (i) the degree of astrocytic soma swelling. (j) The duration of the calcium wave and soma swelling associated with SDs. Data in (b, g, h and e) are expressed as mean ± stdev; individual values are shown in dot plots. A Shapiro-Wilk test was used to evaluate the normal distribution of the data (b, p = 0.494; G, p = 0.050*; h, p = 0.204; i, p = 0.050*). Statistical analysis relied on a one-way ANOVA followed by a Sidak post hoc test (b, p < 0.01** vs. aCSF, p < 0.01## vs. HM_{100}; G, <0.01** vs. Control, p < 0.01## vs. DW), an independent samples T test (H, p < 0.05* and p < 0.01**), or a Mann-Whitney test (I, p < 0.01** vs. Ca; p < 0.01## vs. saline) and a one-tailed Pearson correlation analysis (c).

brain slice recordings testifying that SiD in HM was preceded with an SD1 much longer than SD1 in aCSF (Suppl. Figure 6). Finally, to reverse the effects of water intoxication induced brain swelling, we administered mannitol. Mannitol prevented SiD: the terminal event initiated by oxygen withdrawal was a propagating SD event (4 of 4 experiment, Figure 6(e)), rather than an SiD after water intoxication alone (Figure 6 (D_2)). Also, mannitol treatment shortened the duration of KCl evoked SDs (31.5 ± 8.8 vs. 97.4 ± 42.3 s, DW+mannitol vs. DW) (Figure 6(h)).

We also visualized astrocyte swelling (SR-101) and astrocyte Ca^{2+} dynamics (Fluo-4, AM) in anesthetized mice (Figure 6(f) and (g)). We found that astrocyte somata became swollen 5-10 min after DW intoxication (in contrast with the level baseline in the control group), without detectable intracellular Ca^{2+}

accumulation. Then, a KCl-triggered SD caused remarkable transient astrocyte swelling with a matching, sharp rise of intracellular Ca^{2+}. The SD-related astrocyte swelling was superimposed on the initial swelling caused by DW intoxication. The maximum surface area (cross sectional area, %) of selected astrocyte somata was significantly greater in the DW group (160.47 ± 12.29 vs. 134.85%, water intoxication vs. control) (Figure 6(i)). The SD-related astrocyte swelling and intracellular Ca^{2+} accumulation lasted considerably longer in the DW group (soma swelling: 279.2 ± 44.9 vs. 159.4 ± 23.3 s, water intoxication vs. control; Ca^{2+} peak: 123.3 ± 17.1 vs. 33.0 ± 8.7 s, water intoxication vs. control) (Figure 6(j)). Finally, in contrast with full recovery seen in the control group, neither astrocyte soma volume, nor the intracellular concentration of Ca^{2+} recovered to pre-SD level in the DW

group (Figure 6(j)). We suggest that the duration of astrocyte swelling corresponded to the ability of the tissue to recover from SD. To conclude, we postulate that irreversible astrocyte swelling and dysfunction played a key role in the sequence of events leading to SiD evolution.

Discussion

The key findings of this study are summarized as follows. Cerebral edema produced experimentally is a sufficient condition for SD to occur spontaneously, which predisposes the tissue covered by the propagating SD for an upcoming simultaneous depolarization (SiD). The tissue volume engaged in the SiD then serves as an extensive focus of an SD event taking off from its perimeter. In particular, SiD is predicted by the swelling of astrocytes in edematous tissue. Astrocyte swelling under hypo-osmotic stress is implicated in the excessive extracellular accumulation of glutamate, coincident with SiD occurrence. Further, SiD is followed by the oncotic cell death of neurons and astrocytes, suggestive of injury maturation associated with SiD. Finally, hyperosmotic intervention reduces the susceptibility of the nervous tissue to SD, and fully prevents the cascade of events leading to SiD.

This is the first study to characterize SiD comprehensively. An early review by Marshall (1959) did raise the possibility of SiD encompassing the entire cortex, but without providing any supportive experimental evidence.[42] SiD-like events were later recorded in *ex vivo* brain slice preparations incubated in hypo-osmotic medium and challenged with hypoxia or in response to the bath application of supraphysiological concentration NMDA, but without detailed analysis of the phenomenon or realizing its significance.[43,44] It is of high importance that an SiD-like event has been recently captured in the severely injured human brain.[45] In the ischemic penumbra of a malignant hemispheric stroke, terminal depolarization in the wake of circulatory arrest was seen to arrive with an unusual short delay from electrode to electrode on the subdural strip, when the strip was positioned at an already compromised area of the cortex (Suppl. Figure 7). This observation suggests that SiD is clinically relevant, and gives ample momentum to study the pathophysiological relevance of SiD in more detail. Future clinical studies may attempt to associate particular patterns of SD occurrence with brain edema formation. It is conceivable that edema formation coincident with recurrent SDs leads to irreversible SiD, which seems to represent the conversion of tissue at risk of injury to the infarcted region beyond rescue.

The *ex vivo* brain slice preparations here were exposed to severe osmotic stress achieved by the lowering of $[Na^+]$ of the incubation medium to 100 or 60 mM.[46] This was considered as a model system to study the mechanisms of SiD, rather than the faithful reproduction of a complex disease state. There is no proof that osmotic stress of such severity may occur focused to a discrete site of injury in the human brain. Yet, $[Na^+]_e$ may drop locally to 50-70 mM with SD.[47]

SiD in our study occurred invariably superimposed on tissue edema, a condition to affect astrocytes first. The attention to astrocytes was also substantiated by our finding that fluorocitrate treatment reproduced SiD evolution in brain slices. Astrocytes are more permeable to water than neurons because astrocytes are endowed with AQP-4 water channels at their processes, which conduct osmotically driven water.[48,49] Further, astrocytes have been found to swell in response to ischemia or SD, which is thought to represent water movement via AQP-4 along inward K^+ currents.[17,50] Alternatively, neurons and astrocytes are both affected by the SD-related cytotoxic swelling due to excess chloride entry through NKCC cotransporters.[32,50,51] We found that HM-exposed astrocytes were markedly swollen in histological preparations, and that the blockade of AQP-4 channels and NKCCs prevented tissue edema and SiD occurrence under hypo-osmotic stress. These data collectively demonstrate that astrocyte swelling must be central to SiD evolution.

Astrocytic swelling has been implicated in volume regulated glutamate release through glutamate-permeable VRACs.[41,52,53] At the same time, the significant glutamate uptake through astrocytic Na^+- and ATP-dependent EAAT2 is impaired under metabolic stress, which sustains high extracellular glutamate concentration.[54–56] The inhibition of VRACs in our experiments prevented the extracellular accumulation of glutamate, reduced the focal area of depolarization and the likelihood of SiD occurrence. Conversely, EAAT2 blockade alone reproduced the SiD phenotype as seen under HM incubation. The antagonism of AMPA and NMDA receptors was partially effective against SiD, and resulted in multifocal SD evolution. These results suggest that surplus extracellular glutamate of astrocyte origin, in addition to neuronal release, must be implicated in the evolution of SiD. This seems plausible taken that glutamate appears to contribute to SD propagation, although several arguments cast doubt on the role of glutamate as the mediator driving the propagation of the SD wave front.[57–59]

Previous observations suggest that even with only a very low residual blood flow, SD must last longer than 15 min before cell death occurs in the ischemic core.[60] Our histological results suggest that this time span is significantly shortened when astrocytic function is already disturbed before the onset of neuronal

depolarization. Thus, although SD is a primarily neuronal phenomenon, our findings substantiate the outstanding importance of astrocytes as protective guarantors against the devastating effects of SD.[13,61–63]

The clinical management of cerebral edema in acute brain injury currently aims at the reduction of intracranial pressure and the maintenance of cerebral perfusion pressure by sedation, hyperventilation, osmotherapy, hypothermia, and in the most severe cases decompressive craniectomy.[64–66] However, for example, in severe subarachnoid hemorrhage intravenous high sodium fluids are administered increasingly more frequently because hypoosmolarity is suggested to increase the risk and severity of delayed ischemic injury.[67] Our results that preventive hyperosmotic intervention reduced the excitability of the nervous tissue and most importantly, averted SiD, provide pathophysiological insight into this empirical clinical strategy for the first time, and emphasize the need to invent new ways of preventive osmotherapy in the treatment of acute brain injury.

Declaration of conflicting interests

The author(s) declared no potential conflicts of interest with respect to the research, authorship, and/or publication of this article.

Authors' contributions

ÁM, RF and EF designed the study; ÁM, RF, AEF and OIK conducted experiments, ÁM, RF, AEF, ZS, VÉV, ÁNT and JW acquired data; ÁM, RF, VÉV, ÁNT, CLL, ÍS, RT, JPD and EF analyzed data, DZ-S developed instrumentation and software, AM and SM constructed and provided biosensors, IAK, FB, JPD and EF supervised the work, and ÁM, RF, VÉV, JPD and EF wrote the manuscript.

ORCID iDs

Jens P Dreier https://orcid.org/0000-0001-7459-2828
Eszter Farkas https://orcid.org/0000-0002-8478-9664

Supplemental material

Supplemental material for this article is available online.

References

1. Lauritzen M, Dreier JP, Fabricius M, et al. Clinical relevance of cortical spreading depression in neurological disorders: migraine, malignant stroke, subarachnoid and intracranial hemorrhage, and traumatic brain injury. *J Cereb Blood Flow Metab* 2011; 31: 17–35.
2. Dreier JP, Fabricius M, Ayata C, et al. Recording, analysis, and interpretation of spreading depolarizations in neurointensive care: review and recommendations of the COSBID research group. *J Cereb Blood Flow Metab* 2017; 37: 1595–1625.
3. Hartings JA, Shuttleworth CW, Kirov SA, et al. The continuum of spreading depolarizations in acute cortical lesion development: examining Leao's legacy. *J Cereb Blood Flow Metab* 2017; 37: 1571–1594.
4. Klass A, Sanchez-Porras R and Santos E. Systematic review of the pharmacological agents that have been tested against spreading depolarizations. *J Cereb Blood Flow Metab* 2018; 38: 1149–1179.
5. Somjen GG. Mechanisms of spreading depression and hypoxic spreading depression-like depolarization. *Physiol Rev* 2001; 81: 1065–1096.
6. Dreier JP. The role of spreading depression, spreading depolarization and spreading ischemia in neurological disease. *Nat Med* 2011; 17: 439–447.
7. Dreier JP, Lemale CL, Kola V, et al. Spreading depolarization is not an epiphenomenon but the principal mechanism of the cytotoxic edema in various gray matter structures of the brain during stroke. *Neuropharmacology* 2018; 134: 189–207.
8. Mestre H, Du T, Sweeney AM, et al. Cerebrospinal fluid influx drives acute ischemic tissue swelling. *Science* 2020; 367: eaax7171.
9. Kimelberg HK and Kettenmann H. Swelling-induced changes in electrophysiological properties of cultured astrocytes and oligodendrocytes. I. Effects on membrane potentials, input impedance and cell-cell coupling. *Brain Res* 1990; 529: 255–261.
10. Chebabo SR, Hester MA, Aitken PG, et al. Hypotonic exposure enhances synaptic transmission and triggers spreading depression in rat hippocampal tissue slices. *Brain Res* 1995; 695: 203–216.
11. Roper SN, Obenaus A and Dudek FE. Osmolality and nonsynaptic epileptiform bursts in rat CA1 and dentate gyrus. *Ann Neurol* 1992; 31: 81–85.
12. Rossi DJ, Brady JD and Mohr C. Astrocyte metabolism and signaling during brain ischemia. *Nat Neurosci* 2007; 10: 1377–1386.

13. Largo C, Cuevas P, Somjen GG, et al. The effect of depressing glial function in rat brain in situ on ion homeostasis, synaptic transmission, and neuron survival. *J Neurosci* 1996; 16: 1219–1229.

14. Largo C, Ibarz JM and Herreras O. Effects of the gliotoxin fluorocitrate on spreading depression and glial membrane potential in rat brain in situ. *J Neurophysiol* 1997; 78: 295–307.

15. Larrosa B, Pastor J, Lopez-Aguado L, et al. A role for glutamate and glia in the fast network oscillations preceding spreading depression. *Neuroscience* 2006; 141: 1057–1068.

16. Risher WC, Ard D, Yuan J, et al. Recurrent spontaneous spreading depolarizations facilitate acute dendritic injury in the ischemic penumbra. *J Neurosci* 2010; 30: 9859–9868.

17. Risher WC, Croom D and Kirov SA. Persistent astroglial swelling accompanies rapid reversible dendritic injury during stroke-induced spreading depolarizations. *Glia* 2012; 60: 1709–1720.

18. Matsuura T and Bures J. The minimum volume of depolarized neural tissue required for triggering cortical spreading depression in rat. *Exp Brain Res* 1971; 12: 238–249.

19. Verhaegen MJ, Todd MM, Warner DS, et al. The role of electrode size on the incidence of spreading depression and on cortical cerebral blood flow as measured by H2 clearance. *J Cereb Blood Flow Metab* 1992; 12: 230–237.

20. Tang YT, Mendez JM, Theriot JJ, et al. Minimum conditions for the induction of cortical spreading depression in brain slices. *J Neurophysiol* 2014; 112: 2572–2579.

21. von Bornstadt D, Houben T, Seidel JL, et al. Supply-demand mismatch transients in susceptible peri-infarct hot zones explain the origins of spreading injury depolarizations. *Neuron* 2015; 85: 1117–1131.

22. Seidel JL, Faideau M, Aiba I, et al. Ciliary neurotrophic factor (CNTF) activation of astrocytes decreases spreading depolarization susceptibility and increases potassium clearance. *Glia* 2015; 63: 91–103.

23. Bere Z, Obrenovitch TP, Kozak G, et al. Imaging reveals the focal area of spreading depolarizations and a variety of hemodynamic responses in a rat microembolic stroke model. *J Cereb Blood Flow Metab* 2014; 34: 1695–1705.

24. Percie Du Sert N, Hurst V, Ahluwalia A, et al. The ARRIVE guidelines 2.0: updated guidelines for reporting animal research. *J Cereb Blood Flow Metab* 2020; 40: 1769–1777.

25. Menyhart A, Farkas AE, Varga DP, et al. Large-conductance Ca(2+)-activated potassium channels are potently involved in the inverse neurovascular response to spreading depolarization. *Neurobiol Dis* 2018; 119: 41–52.

26. Farkas E, Bari F and Obrenovitch TP. Multi-modal imaging of anoxic depolarization and hemodynamic changes induced by cardiac arrest in the rat cerebral cortex. *NeuroImage* 2010; 51: 734–742.

27. Menyhart A, Zolei-Szenasi D, Puskas T, et al. Age or ischemia uncouples the blood flow response, tissue acidosis, and direct current potential signature of spreading depolarization in the rat brain. *Am J Physiol Heart Circ Physiol* 2017; 313: H328–H337.

28. Vasylieva N, Maucler C, Meiller A, et al. Immobilization method to preserve enzyme specificity in biosensors: consequences for brain glutamate detection. *Anal Chem* 2013; 85: 2507–2515.

29. Yamaguchi M, Wu S, Ehara K, et al. Cerebral blood flow of rats with water-intoxicated brain edema. *Acta Neurochirurgica Suppl* 1994; 60: 190–192.

30. Hertelendy P, Menyhart A, Makra P, et al. Advancing age and ischemia elevate the electric threshold to elicit spreading depolarization in the cerebral cortex of young adult rats. *J Cereb Blood Flow Metab* 2017; 37: 1763–1775.

31. Igarashi H, Huber VJ, Tsujita M, et al. Pretreatment with a novel aquaporin 4 inhibitor, TGN-020, significantly reduces ischemic cerebral edema. *Neurol Sci* 2011; 32: 113–116.

32. Kimelberg HK. Astrocytic swelling in cerebral ischemia as a possible cause of injury and target for therapy. *Glia* 2005; 50: 389–397.

33. Bourke RS, Waldman JB, Kimelberg HK, et al. Adenosine-stimulated astroglial swelling in cat cerebral cortex in vivo with total inhibition by a non-diuretic acylaryloxyacid derivative. *J Neurosurg* 1981; 55: 364–370.

34. Swanson RA and Graham SH. Fluorocitrate and fluoroacetate effects on astrocyte metabolism in vitro. *Brain Res* 1994; 664: 94–100.

35. Spong KE, Chin B, Witiuk KL, et al. Cell swelling increases the severity of spreading depression in locusta migratoria. *J Neurophysiol* 2015; 114: 3111–3120.

36. Gull S, Ingrisch I, Tausch S, et al. Consistent and reproducible staining of glia by a modified Golgi-Cox method. *J Neurosci Meth* 2015; 256: 141–150.

37. Lu L, Hogan-Cann AD, Globa AK, et al. Astrocytes drive cortical vasodilatory signaling by activating endothelial NMDA receptors. *J Cereb Blood Flow Metab* 2019; 39: 481–496.

38. Risher WC, Andrew RD and Kirov SA. Real-time passive volume responses of astrocytes to acute osmotic and ischemic stress in cortical slices and in vivo revealed by two-photon microscopy. *Glia* 2009; 57: 207–221.

39. Kimelberg HK, Rutledge E, Goderie S, et al. Astrocytic swelling due to hypotonic or high K+ medium causes inhibition of glutamate and aspartate uptake and increases their release. *J Cereb Blood Flow Metab* 1995; 15: 409–416.

40. Basarsky TA, Feighan D and MacVicar BA. Glutamate release through volume-activated channels during spreading depression. *J Neurosci* 1999; 19: 6439–6445.

41. Yang J, Vitery MDC, Chen J, et al. Glutamate-Releasing SWELL1 channel in astrocytes modulates synaptic transmission and promotes brain damage in stroke. *Neuron* 2019; 102: 813–827 e816.

42. Marshall WH. Spreading cortical depression of leao. *Physiol Rev* 1959; 39: 239–279.

43. Kreisman NR, Soliman S and Gozal D. Regional differences in hypoxic depolarization and swelling in hippocampal slices. *J Neurophysiol* 2000; 83: 1031–1038.

44. Jarvis CR, Anderson TR and Andrew RD. Anoxic depolarization mediates acute damage independent of

glutamate in neocortical brain slices. *Cereb Cortex* 2001; 11: 249–259.

45. Dreier JP, Major S, Foreman B, et al. Terminal spreading depolarization and electrical silence in death of human cerebral cortex. *Ann Neurol* 2018; 83: 295–310.

46. Frank R, Bari F, Menyhart A, et al. Comparative analysis of spreading depolarizations in brain slices exposed to osmotic or metabolic stress. *BMC Neurosci* 2021; 22: 33.

47. Hansen AJ and Zeuthen T. Extracellular ion concentrations during spreading depression and ischemia in the rat brain cortex. *Acta Physiol Scand* 1981; 113: 437–445.

48. Andrew RD, Labron MW, Boehnke SE, et al. Physiological evidence that pyramidal neurons lack functional water channels. *Cereb Cortex* 2007; 17: 787–802.

49. Nagelhus EA, Mathiisen TM and Ottersen OP. Aquaporin-4 in the central nervous system: cellular and subcellular distribution and coexpression with KIR4.1. *Neuroscience* 2004; 129: 905–913.

50. Wilson CS and Mongin AA. Cell volume control in healthy brain and neuropathologies. *Curr Top Membr* 2018; 81: 385–455.

51. Stokum JA, Gerzanich V and Simard JM. Molecular pathophysiology of cerebral edema. *J Cereb Blood Flow Metab* 2016; 36: 513–538.

52. Jayakumar AR and Norenberg MD. The Na-K-Cl co-transporter in astrocyte swelling. *Metab Brain Dis* 2010; 25: 31–38.

53. Wilson CS, Bach MD, Ashkavand Z, et al. Metabolic constraints of swelling-activated glutamate release in astrocytes and their implication for ischemic tissue damage. *J Neurochem* 2019; 151: 255–272.

54. Szatkowski M, Barbour B and Attwell D. Non-vesicular release of glutamate from glial cells by reversed electrogenic glutamate uptake. *Nature* 1990; 348: 443–446.

55. Rossi DJ, Oshima T and Attwell D. Glutamate release in severe brain ischaemia is mainly by reversed uptake. *Nature* 2000; 403: 316–321.

56. Mahmoud S, Gharagozloo M, Simard C, et al. Astrocytes maintain glutamate homeostasis in the CNS by controlling the balance between glutamate uptake and release. *Cells* 2019; 8: 184.

57. Pietrobon D and Moskowitz MA. Chaos and commotion in the wake of cortical spreading depression and spreading depolarizations. *Nat Rev Neurosci* 2014; 15: 379–393.

58. Enger R, Tang W, Vindedal GF, et al. Dynamics of ionic shifts in cortical spreading depression. *Cereb Cortex* 2015; 25: 4469–4476.

59. Mei YY, Lee MH, Cheng TC, et al. NMDA receptors sustain but do not initiate neuronal depolarization in spreading depolarization. *Neurobiol Dis* 2020; 145: 105071.

60. Luckl J, Lemale CL, Kola V, et al. The negative ultraslow potential, electrophysiological correlate of infarction in the human cortex. *Brain* 2018; 141: 1734–1752.

61. Peters O, Schipke CG, Hashimoto Y, et al. Different mechanisms promote astrocyte Ca2+ waves and spreading depression in the mouse neocortex. *J Neurosci* 2003; 23: 9888–9896.

62. Chuquet J, Hollender L and Nimchinsky EA. High-resolution in vivo imaging of the neurovascular unit during spreading depression. *J Neurosci* 2007; 27: 4036–4044.

63. Dreier JP and Reiffurth C. The stroke-migraine depolarization continuum. *Neuron* 2015; 86: 902–922.

64. Bardutzky J and Schwab S. Antiedema therapy in ischemic stroke. *Stroke* 2007; 38: 3084–3094.

65. Carney N, Totten AM, O'Reilly C, et al. Guidelines for the management of severe traumatic brain injury, fourth edition. *Neurosurgery* 2017; 80: 6–15.

66. Jha RM, Kochanek PM and Simard JM. Pathophysiology and treatment of cerebral edema in traumatic brain injury. *Neuropharmacology* 2019; 145: 230–246.

67. Schupper AJ, Eagles ME, Neifert SN, et al. Lessons from the CONSCIOUS-1 study. *J Clin Med* 2020; 9: 2970.